Matrix Infrared Spectroscopy and a Theoretical Investigation of SUO and US$_2$

Lester Andrews,[a] Xuefeng Wang,[a] Binyong Liang,[a] Fernando Ruipérez,[b] Ivan Infante,*[b] Adam D. Raw,[c] and James A. Ibers[c]

US$_2$ and SUO molecules have been prepared by laser ablation of the solid materials and reaction of the elements during condensation in solid argon, which give the same absorptions as earlier U atom reactions with sulfur vapor and sulfur dioxide. The antisymmetric stretching mode of US$_2$ shifts from 438.7 cm^{-1} in solid argon to 442.3 cm^{-1} in solid neon, which shows that the same electronic state is trapped in both matrix environments. Density functional calculations find a bent ($^3B_2$) ground state for the US$_2$ molecule, and CASSCF/ CASPT2 calculations reveal a multiconfigurational mixture of $(5f\phi)^1(5f\delta)^1$-type states, whereas the most stable state for UO$_2$ is a linear structure of the $(5f\phi)(7s)$ type. The bent triplet ground state SUO molecule exhibits similar multireference character with the U–O stretching mode at 857.1 cm^{-1} in solid argon. The linear SUO molecule computed at the CASPT2 level is only 2 kcal/mol above the bent structure. A detailed analysis of the bonding in US$_2$ and SUO is provided and compared to the better known UO$_2$ molecule.

Introduction

The chemistry of uranium is important; however, the chemistry of significant fundamental gaseous uranium species is a largely neglected area.[1–5] Among the best known, yet still not fully understood, actinide molecules is UO$_2$, which is linear based on oxygen isotopic substitution infrared spectra and theoretical calculations,[2–5] whereas solid UO$_2$ forms cubic crystals.[6] However, US$_2$ forms tetragonal crystals and the US$_2$ molecule is bent as determined from the argon matrix sulfur isotopic infrared spectrum and density functional calculations.[7,8] Solid SUO also forms tetragonal crystals, and the SUO molecule has been detected as a minor product in the reaction of laser-ablated U atoms and SO$_2$.[9,10] This work has two purposes: first, to prepare SUO and US$_2$ molecules for matrix spectroscopic observation using different source materials in order to confirm their previous identification from argon matrix reactions of laser-ablated U atoms, SO$_2$, and elemental sulfur[8,10] and second, to perform high-level calculations on the electronic structures of SUO and US$_2$. Moreover, the UO$_2$ electronic state is believed to change on going from the solid argon to neon matrix environments owing to a stronger interaction with argon than with neon.[3,11] Hence, we also wanted to characterize US$_2$ in a solid neon matrix to compare with the solid argon results.[8]

Another important question to be answered is why the UO$_2$ molecule prefers a linear conformation, whereas US$_2$ undoubtedly has a bent structure. To clarify the origin of the linear structures of actinoids, early computational work by Wadt[12] attempted to demonstrate the linearity of the uranyl UO$_2^{2+}$ ion with respect to the isoelectronic bent ThO$_2$ molecule. His conclusion was that in species where the chemical bond was dominated by the 5f–2pπ orbital interaction, the bond would be linear, as in UO$_2^{2+}$, whereas in species where the 6d–2pπ orbital interaction was dominant, as in ThO$_2$, the bond would be bent. For the same reasons, Tatsumi et al.[13] claimed that that the uranium sulfide species, where the 6d contribution is critical, would be bent. In these earlier studies, however, the nature of the bond is explained using only molecular orbital interaction diagrams between the uranium and the peripheral atoms, and there is no mention of the critical contribution of the Pauli repulsion and the electrostatic interactions in stabilizing the linear or the bent conformations. In this work, we attempt to fill this gap using modern theoretical tools.

Results and Discussion

US$_2$

The codeposition of laser-ablated U atoms with sulfur vapor in excess neon produced weak bands at 686.8, 683.5, and 680.8 cm^{-1}, which are blueshifted 3–4 cm^{-1} from the argon matrix absorptions assigned to the S$_3$ molecule.[14]

[a] Department of Chemistry, University of Virginia,
McCormick Road, P. O. Box 400319, Charlottesville, VA 22904-4319, USA
Fax: +1-434-924-3710
E-mail: lsa@virginia.edu
[b] Kimika Fakultatea, Euskal Herriko Unibertsitatea and
Donostia International Physics Center (DIPC),
P. K. 1072, 20080 San Sebastian, Spain
Fax: +34-943-015270
E-mail: iinfant76@gmail.com
[c] Department of Chemistry, Northwestern University,
Evanston, IL 60208-3113, USA
Fax: +1-847-491-2976
E-mail: ibers@chem.northwestern.edu

The ^{34}S counterparts were observed at 666.4, 663.3, and 660.7 cm^{-1}, which define 32:34 isotopic frequency ratios (1.0306, 1.0305, and 1.0304) in agreement with those observed for the argon matrix isolated species. In the mixed ^{32}S and ^{34}S isotopic experiments a doublet of these matrix site split triplets was observed without any intermediate mixed isotopic components, which indicates that S_3 is probably produced here by photodissociation of the S_8 precursor molecules with UV radiation from the intense laser ablation plume on the surface of the uranium target. Similarly, S_4 absorptions were observed at 665.4 and 646.7 cm^{-1} with ^{34}S isotopic counterparts at 645.8 and 627.4 cm^{-1}, again blueshifted 3–4 cm^{-1} from the argon matrix values,[14] and again no mixed isotopic bands were observed. New product absorptions were observed in the U–S stretching region at 442.3 cm^{-1} for ^{32}S and at 431.5 cm^{-1} for ^{34}S: these bands increased slightly on full mercury arc irradiation and on annealing at 10 and 12 K (Figure 1). Two mixed sulfur isotopic experiments revealed the same bands without any new mixed isotopic components.
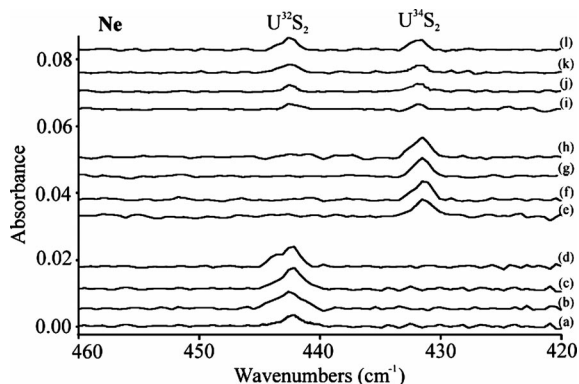

Figure 1. IR spectra of the laser-ablated uranium and thermal sulfur S_8 vapor reaction products in the 460–420 cm^{-1} region trapped in solid neon. (a) Laser-ablated U and natural isotopic S_8 codeposited in excess neon at 5 K for 60 min, (b) after > 220 nm irradiation for 20 min, (c) after annealing to 10 K, and (d) after annealing to 12 K. (e) Laser-ablated U and 98% enriched isotopic $^{34}S_8$ codeposited in excess neon at 5 K for 60 min, (f) after > 220 nm irradiation for 20 min, (g) after annealing to 10 K, and (h) after annealing to 12 K. (i) Laser-ablated U and 50:50 mixed isotopic $^{32}S_8$ and $^{34}S_8$ codeposited in excess neon at 5 K for 60 min, (j) after > 220 nm irradiation for 20 min, (k) after annealing to 10 K, and (l) after annealing to 12 K.

These bands are blueshifted 3.6 and 3.7 cm^{-1} from the argon matrix bands, 438.7 and 427.8 cm^{-1}, assigned to sulfur isotopic counterparts of the SUS molecule.[8] Furthermore, the 32:34 isotopic frequency ratio (1.0250) is in agreement with that observed for the argon matrix isolated species (1.0255), which substantiates assignment of the neon matrix bands to SUS. Unfortunately the yield is too low to observe the weaker symmetric stretching mode observed at 449.8 cm^{-1} in solid argon.[8] The SUS molecule is probably prepared here in the same reaction as in previous sulfur discharge argon matrix experiments,[8] but here S_2 is likely produced by photodissociation of S_8 by the intense laser ablation plume [Equation (1)].

$$U + S_2 \rightarrow SUS \tag{1}$$

The solid US$_2$/S target was ablated into freezing neon in two experiments, but no new bands were detected in the low signal to noise 450 cm^{-1} region. However, trapping in solid argon gave the strong US$_2$ band at 438.8 and the weaker band at 449.9 cm^{-1}, as shown in Figure 2, and reproduced in a second experiment. Annealing sharpened these bands, but UV irradiation had no effect. In addition, S_3 bands were observed at 676.2 and 680.1 cm^{-1} (0.01 absorbance). UO and UO$_2$ were detected (0.002 absorbance), and the sharp 857.1 cm^{-1} band, previously assigned to SUO,[10] appeared as shown in Figure 3 (e) and increased on subsequent annealing.
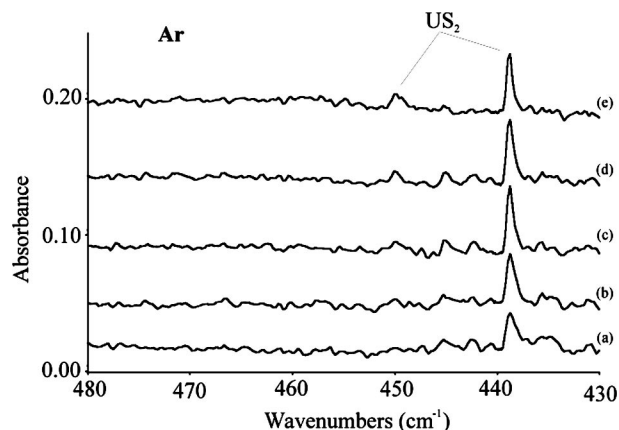

Figure 2. IR spectra of products from laser-ablated solid US$_2$/S in the 480–430 cm^{-1} region trapped in solid argon. (a) Laser-ablated solid US$_2$/S products trapped in solid argon at 5 K for 60 min, (b) after annealing to 20 K, (c) after annealing to 30 K, (d) after > 220 nm irradiation for 20 min, and (e) after annealing to 35 K.
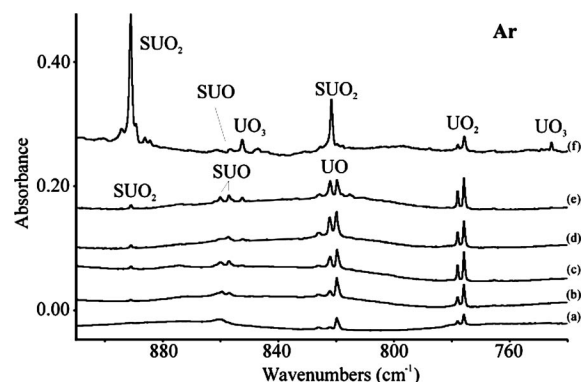

Figure 3. IR spectra of products from laser-ablated solid SUO/S in the 900–740 cm^{-1} region trapped in solid argon. (a) Laser-ablated solid SUO/S products trapped in solid argon at 5 K for 60 min, (b) after annealing to 20 K, (c) after annealing to 30 K, and (d) after > 220 nm irradiation for 20 min, and (e) after annealing to 35 K. (f) Laser-ablated U and SO$_2$ codeposited in excess argon, after > 220 nm irradiation and annealing to 30 K from Ref.[10]

We carried out theoretical calculations at different levels of theory to provide further insights into the infrared spectrum of the US$_2$ molecule. In Table 1, we give the structural

properties and the vibrational frequencies of the US$_2$ molecule computed using two exchange-correlation functionals within the DFT framework: PBE and PBE0.[15] The ground state (GS) is a triplet state, $^3B_2$, bent molecule with C_{2v} symmetry, as reported earlier.[8] The PBE0 provides a shorter U–S bond length compared to PBE and a smaller S–U–S angle. The asymmetric stretch is computed at 462 (PBE0) and 441 cm^{-1} (PBE), which are in good agreement with the experiment, 439 (in argon) or 442 cm^{-1} (in neon), and previous DFT values.[8] In addition, we performed CASSCF/CASPT2 calculations,[16,17] which show some peculiar features and are presented below, in Table 1. As evidenced by the data in Table 2, the triplet ground state is not composed of one single configuration state function (CSF), but it is a linear combination of at least two configurations whose weight is 66 and 29%.

Table 1. Predicted geometrical parameters and vibrational stretching frequencies computed at the CASPT2, DFT/PBE/TZ2P, and DFT/PBE0/TZ2P level of theory of the optimized SUO and US$_2$ molecules for a given method.

	DFT/PBE	DFT/PBE0	CASPT2	Experiment
US$_2$				
U–S	2.351	2.331	2.365	–
S–U–S	120	114	122	–
ν_s	423	465	489	not obs [Ne] 450 [Ar]
ν_{as}	441	462	488	442 [Ne] 439 [Ar]
SUO				
U–S	2.347	2.386	2.374	–
U–O	1.811	1.815	1.849	–
S–U–O	180	126	121	–
ν_s	412/414	437	466	–
ν_{as}	859/833	869	847	871 [Ne] 857 [Ar]

Table 2. Orbital composition for the spin-free ground state of the SUO and US$_2$ molecules computed at the CASSCF/CASPT2 level of theory.

Composition	
SUO ($^3A'$)	67% $(5f\phi_-)^1(5f\delta_+)^1$ + 25% $(5f\phi_+)^1(5f\delta_-)^1$
($5f\phi_-$)	93% $5f\phi_-$ + 3% $6d\delta_+$ + 2% $2p$ O
($5f\delta_+$)	90% $5f\delta_+$ + 6% $6d\pi$ + 1% $5f\sigma$ + 1% $2p$ O
($5f\phi_+$)	89% $5f\phi_+$ + 6% $5f\delta_-$ + 3% $6d\pi_-$ + 2% $5f\pi_+$
($5f\delta_-$)	87% $5f\delta_-$ + 6% $5f\phi_+$ + 6% $6d\pi_+$
US$_2$ ($^3B_2$)	66% $(5f\phi_-)^1(5f\delta_+)^1$ + 29% $(5f\phi_+)^1(5f\delta_-)^1$
($5f\phi_-$)	93% $5f\phi_-$ + 4% $5f\pi_-$ + 3% $6d\delta_+$
($5f\delta_+$)	87% $5f\delta_+$ + 9% $5f\sigma$ + 6% $6d\pi_-$
($5f\phi_+$)	96% $5f\phi_+$ + 2% $5f\pi_+$ + 2% $6d\pi_-$
($5f\delta_-$)	96% $5f\delta_-$ + 3% $6d\pi_+$

Looking at the composition of both of these CSFs, we notice that the two unpaired electrons are localized in molecular orbitals mainly composed of the $5f\phi$ and $5f\delta$ nonbonding atomic orbitals. However, unlike the linear structure, the bent conformation allows mixing between 5f and 6d orbitals so that the nonbonding $5f\phi$ and $5f\delta$ can mix with the $6d\pi$ and $6d\delta$ orbitals. The composition of the US$_2$

ground state differs from the ground state found for UO$_2$, where the most stable state is a linear structure of the $(5f\phi)(7s)$ type. In this latter molecule the $(5f\phi)(5f\delta)$ state lies at much higher energies. The fact that the GS is multiconfigurational could suggest that DFT may have problems in correctly describing some of the molecular properties, in particular the energy of excited states. However, in this work we are mostly interested in the geometrical parameters of the ground state, which are correctly described using DFT. The CASPT2 structure shows a U–S bond length of 2.365 Å, slightly larger than the DFT value, and an angle of about 120°. The asymmetric vibrational stretching mode computed at 488 cm^{-1} is somewhat larger than the experimental value of 439 cm^{-1}, but still within reasonable agreement. Of particular interest is the weaker symmetric stretch, which, as evidenced earlier, appears in the argon matrix,[8] but not in the lower yield solid neon experiments. At the DFT/PBE0 and CASPT2 levels of theory this vibration lies very close, within 1–3 cm^{-1}, to the antisymmetric stretch. This suggests that the weaker band might overlap with the more intense band. In an argon matrix, the host can interact with the trapped US$_2$ molecule giving the possibility of resolving the two vibrational stretching modes. Evidence for strongly interacting matrices on the electronic structure of trapped molecules has been given in an earlier study on the UO$_2$ molecule.[11]

SUO

The ablated material from the solid SUO/S target was codeposited with excess argon using two different laser energies, and infrared spectra of the better experiment are shown in Figure 3. The initial deposited sample revealed UO and UO$_2$ absorptions[2] and a broad 860 cm^{-1} band, trace (a). Annealing sharpened the latter into a sharp 860.1, 857.1 cm^{-1} doublet and produced the strongest SUO$_2$ band at 891.1 cm^{-1} and weak UO$_3$ absorptions.[2,10] Weak S$_3$ bands were observed, and no US$_2$ was detected. The 857.1 cm^{-1} band is in excellent agreement with a weak 857.0 cm^{-1} band assigned to the SUO molecule produced in the U/SO$_2$ reaction in excess argon.[10]

The experimental infrared spectrum does not provide a basis to determine whether the SUO molecule is bent or linear. DFT/PBE and DFT/PBE0 results are shown in Table 1, along with the CASPT2 values. All three methods provide a triplet state as the ground state; however, some geometrical differences are found. For example, DFT/PBE0 and CASPT2 show a bent structure, whereas DFT/PBE converges to a linear structure. This difference can be assigned to the small energy gap between the two structures. At the CASPT2 level, the bent structure is only 2 kcal/mol more stable than the linear one, whereas at the DFT/PBE level the bent structure is just slightly less stable than the linear one (at DFT/PBE0 the bent exhibits the same CASPT2 energy gap). In Table 3 we give an overview of the main energy differences between the two conformations, linear and bent, computed for different electronic states.

The notable feature is that the linear $(5f\phi)(7s)$ state becomes steadily destabilized from UO_2 to US_2, whereas the $(5f\phi)(5f\delta)$ state becomes more stabilized breaking the linear structure and favoring a bent conformation. In the next section we will give more details about the reasons why each of the species has a different geometry.

Table 3. Energy differences [kcal/mol] between linear and bent structures for the UO_2, SUO, and US_2 molecules obtained at the DFT/PBE/TZ2P level of theory and relative to the most stable states for each species. Note that at CASPT2 and DFT/PBE0 level of theory, the SUO exhibits the bent structure as the more stable. We listed the DFT/PBE values because the energy decomposition has been carried out using this exchange-correlation functional.

Type	UO_2	SUO	US_2
Linear			
$(5f\phi)(7s)$	0.0	8.7	14.4
$(5f\phi)(5f\delta)$	14.9	0.0	14.2
Bent			
$(5f\phi)(5f\delta)$	8.8	1.6	0.0

The experimental band of the SUO molecule at 857 cm^{-1} matches reasonably well with our calculated vibrational stretch of the U–O bond: 859 (PBE), 869 (PBE0), and 847 cm^{-1} (CASPT2). As in the case of US_2, the ground state of the SUO molecule shows multireference character formed by a linear combination of two CSFs whose weight is 67 and 25% (see Table 2 for more details).

Bent or Linear?

A consideration of the crystal structures of the corresponding solids affords a qualitative explanation for the linear structure of UO_2 and the bent nature of US_2. In cubic UO_2[6] the U^{4+} cation (crystallographic site symmetry $m3m = O_h$) is surrounded by eight O^{2-} anions at the corners of a tetragonal bipyramid. The shortest O···O distance is 2.73 Å, which is about twice the ionic radius of four-coordinate O^{2-} (1.38 Å).[18] Thus, there is no hint of O–O interactions. In contrast, in tetragonal US_2[19] one independent U^{4+} ion (site symmetry $42 = D_4$) is surrounded by eight S^{2-} ions at the corners of a bicapped trigonal prism and the other independent U^{4+} ion (site symmetry $mm = C_{2v}$) is surrounded by seven S^{2-} ions at the corners of a seven-vertex polyhedron. In the former, the shortest S···S distance is 3.16 Å, whereas in the latter it is 3.06 Å. These are both longer than a typical S–S single bond length of 2.06 Å, but are markedly shorter than twice the ionic radius of S^{2-} (1.84 Å)[18] and are indicative of S–S interactions. This is in keeping with the well known tendency of the chalcogens to form chains, rings, and other moieties arising from such interactions. One can thus look upon solid US_2 as containing incipient bent US_2 molecules arising from S–S interactions. This qualitative approach does not afford an insight into whether the SUO molecule is linear or bent. In solid SUO[9] the U^{4+} ion (site symmetry $4mm = C_{4v}$) is surrounded by five O^{2-} ions and four S^{2-} ions at the corners of a distorted monocapped square antiprism. The shortest S···O distance is 3.11 Å, which is slightly shorter than the sum of the individual ionic radii (3.22 Å).

For a more quantitative approach to the question of conformations, we decomposed the XUY molecule into two interacting fragments: the peripheral X···Y moiety (X···Y can be O···O, S···O or S···S) and the U atom, both of them computed as neutral species. Under this framework, unfortunately, we do not have any direct information on the interaction between the two peripheral atoms, because they are both considered inside a single fragment. The fragment decomposition approach, originally presented by Ziegler and Rauk,[20] allows a partition of the bond energy into several components of chemical relevance: Pauli repulsion, electrostatic interaction, and orbital interaction, the latter including both charge transfer and polarization effects. In all three molecules, the bond energy decomposition occurs between two fragments that for computational reasons had to be calculated in a restricted open-shell fashion (the ADF program does not allow direct computation of the interaction energy between two unrestricted open-shell moieties). As expected, both the fragments present a significant spin polarization (i.e. the energy needed to bring the molecule from an unrestricted open-shell electronic configuration to a restricted open-shell one): the uranium atom has a known quintet ground state, and the O···O, S···O, and S···S moieties are computed also as quintet states. These latter species, when found in their most stable geometrical conformation, present triplet ground states, but their bond separation in the fragment moiety X···Y is about 3.5–4.0 Å, in such a way that we can consider them as two separate atoms. This leads to two coupled triplet states that give an overall quintet state. Under this framework, we computed the spin polarization as a separated term, called preparation energy, Δ_{prep}, which is always positive, as it implies forcing the alpha and beta electrons to share the same molecular orbital.

In this analysis (see Table 4), we can firstly compare the decomposition energies of the linear $[(5f\phi)(7s)]$ UO_2 with the linear SUO and US_2 molecules. The same conclusions on their trend can be drawn from comparing the linear $[(5f\phi)(5f\delta)]$ or the bent species. The Pauli repulsion term is much higher for the UO_2 molecule and decreases along the series, SUO and US_2. This can be explained by the fact that the oxygen atoms in UO_2 are closer than the sulfur atoms in US_2, hence the O···O electronic cloud largely overlaps with the uranium center, yielding a strong repulsive effect. On the other hand, sulfur is rather diffuse hence the electrons are more widely delocalized, especially in regions outside the bond with the uranium, providing a weaker Pauli repulsion. The electrostatic interaction is more attractive in UO_2, but this effect is not as large as the Pauli term. Indeed, the Pauli repulsion decreases by about 466 kcal/mol from UO_2 to US_2, but the electrostatic interaction is reduced by only 108 kcal/mol (Table 4). Hence, the steric interaction (the sum of Pauli and Electrostatic terms) is most destabilizing for linear UO_2. On the other hand, the orbital interaction term overcomes such a repulsive effect leaving UO_2 as the molecule with the strongest bonding interaction. The charge transfer of 2.33 e from uranium to

Table 4. Bond energy decomposition [kcal/mol] of the interaction between the peripheral X···Y [XY = O–O, S–O, S–S] moiety and the uranium atom for the XUY molecule. These values have been obtained at the DFT/PBE/TZ2P level of theory. The SUO and US$_2$ geometries have been optimized for each given electronic structure. Only in the case of UO$_2$, the bent geometry has been selected arbitrarily, with the same bond length as the linear ground state and a forced bent 120° angle. This was done because no local minimum was found for the bent conformation of UO$_2$.

	UO$_2$	SUO	US$_2$
Linear (5fϕ)(7s)			
Pauli repulsion	1539.1	1301.9	1073.0
Electrostatic interaction	−562.8	−512.1	−454.5
Steric interaction	976.3	789.9	618.5
Orbital interaction	−1400.8	−1143.8	−895.5
Total interaction	−424.5	−354.0	−277.1
Δ_{prep}	12.9	11.4	9.3
Charge transfer	2.33	2.20	1.99
Total bonding energy	−411.6	−342.6	−267.8
Linear (5fϕ)(5fδ)			
Pauli repulsion	1539.1	1269.8	931.8
Electrostatic interaction	−562.8	−498.7	−393.4
Steric interaction	976.3	771.1	538.4
Orbital interaction	−1386.0	−1133.7	−815.7
Total interaction	−409.6	−362.7	−277.3
Δ_{prep}	12.9	11.4	9.3
Charge transfer	2.55	2.52	2.42
Total bonding energy	−396.7	−351.3	−269.0
Bent			
Pauli repulsion	1444.3	1130.4	920.0
Electrostatic interaction	−505.0	−433.7	−387.5
Steric interaction	939.3	696.7	532.5
Orbital interaction	−1355.4	−1058.1	−824.5
Total interaction	−416.2	−361.4	−292.0
Δ_{prep}	13.4	11.7	9.8
Charge transfer	2.42	2.39	2.27
Total bonding energy	−402.8	−349.7	−282.2

the oxygen atoms is somewhat larger than that found in SUO (2.20 e) and US$_2$ (1.99 e). However, only the charge transfer cannot explain the huge difference in the orbital interaction energy within UO$_2$ (−1400.8 kcal/mol) and, for example, US$_2$ (−895.5 kcal/mol). The orbital interaction term, however, includes pair bond formation, and mostly, charge rearrangement within each fragment. These latter two terms, which cannot be quantified into separate contributions in our analysis, are most probably responsible for these large orbital interaction differences. To further corroborate the effect of the charge transfer, and particularly the charge rearrangement, we have computed natural population charges for each given species (see Table 5 for details).

In order to explain why the UO$_2$ molecule prefers the linear conformation, we can look at the decomposition energy of both the linear and bent species. The first notable feature is the reduction of the Pauli repulsion on going from the linear to the bent structure. This can be explained intuitively by the fact that the maximum repulsion is obtained along the axis of the linear molecule and distortion from linearity partially relieves this effect. This damping of the Pauli repulsion is about 100 kcal/mol (from 1539.1–1444.3 kcal/mol). The electrostatic term is also reduced (the

Table 5. Natural population charges and natural population configurations computed at DFT/PBE/TZ2P level of theory for each atom in a given molecular species.

Atomic Electronic Configuration			
U	(7s)$^{2.0}$(6d)$^{1.0}$(5f)$^{3.0}$		
O	(2s)$^{2.0}$(2p)$^{4.0}$		
S	(3s)$^{2.0}$(3p)$^{4.0}$		
Natural population analysis UO$_2$			
	Linear (5fϕ)(7s)	Linear (5fϕ)(5fδ)	Bent
U	(7s)$^{0.94}$(6d)$^{0.41}$(5f)$^{2.43}$	(7s)$^{0.06}$(6d)$^{0.37}$(5f)$^{3.09}$	(7s)$^{0.51}$(6d)$^{0.60}$(5f)$^{2.47}$
O	(2s)$^{1.98}$(2p)$^{5.14}$(3d)$^{0.03}$	(2s)$^{1.98}$(2p)$^{5.26}$(3d)$^{0.03}$	(2s)$^{1.98}$(2p)$^{5.19}$(3d)$^{0.03}$
Natural population analysis SUO			
U	(7s)$^{0.82}$(6d)$^{0.56}$(5f)$^{2.50}$	(7s)$^{0.06}$(6d)$^{0.45}$(5f)$^{3.02}$	(7s)$^{0.36}$(6d)$^{0.49}$(5f)$^{2.39}$
O	(2s)$^{1.98}$(2p)$^{5.13}$(3d)$^{0.03}$	(2s)$^{1.98}$(2p)$^{5.14}$(3d)$^{0.03}$	(2s)$^{1.98}$(2p)$^{5.14}$(3d)$^{0.03}$
S	(3s)$^{1.99}$(3p)$^{5.01}$(4d)$^{0.05}$	(3s)$^{1.99}$(3p)$^{5.23}$(4d)$^{0.05}$	(3s)$^{1.99}$(3p)$^{5.14}$(4d)$^{0.05}$
Natural population analysis US$_2$			
U	(7s)$^{0.81}$(6d)$^{0.71}$(5f)$^{2.53}$	(7s)$^{0.01}$(6d)$^{0.55}$(5f)$^{3.05}$	(7s)$^{0.22}$(6d)$^{0.55}$(5f)$^{3.05}$
S	(3s)$^{2.00}$(3p)$^{4.96}$(4d)$^{0.04}$	(3s)$^{2.00}$(3p)$^{5.17}$(4d)$^{0.05}$	(3s)$^{2.00}$(3p)$^{5.10}$(4d)$^{0.04}$

maximum attraction is still obtained when the molecule is linear), but in a less extensive way (from −562.8 to −505.0 kcal/mol). Combining these two contributions, we obtain an overall steric interaction less repulsive by 37.0 kcal/mol for the bent molecule (939.3 vs. 976.3 kcal/mol). Regarding the orbital interaction term, the linear molecule obtains an overall relaxation of the electron density from the isolated fragments, which is more stabilizing (45.4 kcal/mol) with respect to the bent structure. This contribution overturns the relative stabilization of the two conformers, causing the linear structure to be more stable.

Moving to the US$_2$ molecule, we find the steric interaction in the bent structure less repulsive by about 86 kcal/mol than the linear molecule (532.5 vs. 618.5 kcal/mol). This is quite striking compared to the UO$_2$ molecule where the linear/bent difference in the steric term was only 37.0 kcal/mol. This effect is mostly driven by the large reduction of Pauli repulsion from the linear to the bent conformation of about 153 kcal/mol (100 kcal/mol in UO$_2$). The orbital interaction term still favors the linear structure, however, not enough to overturn the overall stabilization of the bent structure. Indeed, the orbital relaxation stabilizes linear US$_2$ by 71 kcal/mol, somewhat similar to that obtained for UO$_2$, (85.4 kcal/mol), but still smaller than the steric interaction that prefers the bent form. In conclusion, for US$_2$ the relief of Pauli repulsion going from linear to bent helps to keep the bent structure more stable, despite the fact that orbital interaction favors the linear conformation.

In SUO the situation is intermediate between the UO$_2$ and US$_2$. The most stable structure at DFT/PBE level is the linear (5fϕ)(5fδ) state by just 1.6 kcal, hence the comparison is made with respect to this state. The steric interaction is less repulsive in the bent structure by 65.0 kcal/mol, whereas the orbital interaction favors the linear structure by 75.6 kcal/mol. This makes the linear structure more stable, but the energy difference remains small. At the

CASPT2 level, this energy gap is only 2 kcal/mol and well within the error of the computational method (DFT/PBE0 gives the same value as CASPT2).

Conclusions

Laser ablation and matrix isolation spectroscopy have been used to produce US_2 and SUO molecules in solid argon using new methods. The asymmetric stretching mode of US_2 is found at 438.7 cm^{-1}, about 4 cm^{-1} lower than in solid neon. Unlike the UO_2 molecule, there is no ground state reversal in changing the matrix environment. The SUO molecule exhibits a U–O stretching mode at 857.1 cm^{-1}, in agreement with the DFT and CASPT2 calculations that compute the ground state as a bent triplet structure. Theoretical results also show that US_2 presents a bent triplet ground state, which has a multiconfigurational nature of mainly two configuration state functions. A similar multireference character is found for SUO. From the fragment decomposition above we find that the linear structure is favored in UO_2, and the bent structure is favored in US_2.

Experimental Section

General: Laser-ablated U atoms were treated with S_8 mixtures in neon during condensation at 5 K using methods described in our previous papers.[8,10,14,21,22] Natural isotopic sulfur (Electronic Space Products, Inc.), enriched sulfur (98% ^{34}S, Cambridge Isotope Laboratories), and different mixtures of the two isotopic samples were also employed. The vapor pressure of sulfur feeding the deposition tube was controlled by resistance heating of the sample reservoir. The Nd:YAG laser fundamental (1064 nm, 10 Hz repetition rate with 10 ns pulse width) was focused onto a rotating uranium target (Oak Ridge National Laboratory, high purity, depleted of ^{235}U). FTIR spectra were recorded at 0.5 cm^{-1} resolution with a Nicolet 750 with 0.1 cm^{-1} accuracy using an HgCdTe range B detector.

Several microwave discharge experiments were performed with neon in the previous apparatus using a 5 K substrate,[14] but the discharged effluent provided too much heat for the surface to condense neon effectively. However, similar neon experiments were performed without discharge, and the deposited samples revealed infrared spectra of new reaction products.

A sample of solid SUO synthesized as described[9] was pressed into a 1/4 inch dia pellet, which was not cohesive enough to handle, but 10 English tons of pressure applied to this material premixed with half again more elemental sulfur formed the pellet used for laser ablation and trapping in solid argon. Similarly, a sample of pressed solid US_2 did not hold together, but mixing with half again more sulfur enabled a usable laser ablation target to be prepared using 10 English tons of pressure.

Computational Details

All ab initio calculations were performed using the complete active space CASSCF method[16] followed by multiconfigurational second-order perturbation theory (CASPT2).[17] Scalar relativistic effects were included using the Douglas–Kroll–Hess Hamiltonian[23] and relativistic ANO-RCC basis set[24] of VTZP quality implemented in the MOLCAS 7.4 package.[25] In the CASSCF treatment, the ideal active space of US_2 and SUO was composed of 19

orbitals, 13 of which come from a linear combination of the 5f, 6d, and 7s orbitals of the uranium atom and the remaining six from the 3p orbitals of the sulfur atom (or 2p orbitals for the oxygen atom). This means that the active space would contain 14 electrons, i.e. six valence electrons from the uranium and eight valence electrons from the two peripheral atom 3p (or 2p) orbitals. Unfortunately, an active space of (14e/19o) is computationally unfeasible owing to the large number of configuration state functions involved. We thus decided to make a consistent truncation of the space by removing the two lowest ($6d\pi_g$–$2p_{x,y}$) bonding orbitals and the corresponding antibonding orbitals. This yields a more affordable space of (10e/15o). Test calculations have also shown that a smaller active space, (8e/13o), gives results in good agreement with the larger (10e/15o),[11] hence we decided to proceed with this smaller CAS for computational advantage. In this new CAS we removed the bonding ($6d\sigma_g$–$2p_z$) and its antibonding combination. This active space is similar to that chosen by Infante et al.[11] At this level of theory we applied the C_{2v} symmetry for the US_2 molecule and C_s for the linear and bent SUO. We performed geometry optimizations and numerical second order derivatives to retrieve the vibrational frequencies of each given species. This approach has been successful in studying many actinide-containing systems.[11,26]

We have also performed calculations using DFT, employing the PBE correlation-exchange (xc) functional[15] as it has been proven to provide similar results to the CASPT2.[11] A TZ2P basis-set was used for all computed optimized geometrical structures and vibrational frequencies.

In addition, we have carried out a fragment decomposition analysis[20] using the ADF2009 program[27] to study the interaction between the U atom and the peripheral S_2 moiety within the US_2 molecule or between U and SO moieties within SUO. The bonding energy between the two fragments at the equilibrium is expressed as the sum between two terms: the first contribution is a stabilizing term called δE_{int}, which includes the interaction between restricted closed-shell/open-shell densities of the two fragments. δE_{int} is itself decomposed into three quantities that have a direct physical meaning: the Pauli repulsion, the electrostatic interaction, and the orbital interaction (includes the polarization and the charge transfer effects) between the two moieties. The second term is usually a small spin polarization term, ΔE_{SP}, which is the energy difference between the individual spin polarization term, E_{SP}, of each molecular fragment. The E_{SP} contribution is always positive as it is the deformation of the electron density from a relaxed unrestricted open-shell density to a restricted closed-shell one. The ΔE_{SP} can be either positive or negative depending on how each fragment contributes to the spin polarization.

Acknowledgments

[1] a) R. D. Hunt, J. T. Yustein, L. Andrews, *J. Chem. Phys.* **1993**, *98*, 6070 (UN$_2$). b) L. Andrews, X. F. Wang, R. Lindh, B. O. Roos, C. J. Marsden, *Angew. Chem. Int. Ed.* **2008**, *47*, 5366.

[2] a) S. D. Gabelnick, G. T. Reedy, M. G. Chasanov, *J. Chem. Phys.* **1973**, *58*, 4468 (UO, UO₂ in argon). b) R. D. Hunt, L. Andrews, *J. Chem. Phys.* **1993**, *98*, 3690 (UO, UO₂ and UO₃ in argon).

[3] M. F. Zhou, L. Andrews, N. Ismail, C. Marsden, *J. Phys. Chem. A* **2000**, *104*, 5495–5502 (UO₂ in solid neon).

[4] L. Gagliardi, B. O. Roos, *Chem. Phys. Lett.* **2000**, *331*, 229.

[5] L. Gagliardi, B. O. Roos, P. A. Malmqvist, J. M. Dyke, *J. Phys. Chem. A* **2001**, *105*, 10602.

[6] R. E. Rundle, N. C. Baenziger, A. S. Wilson, R. A. McDonald, *J. Am. Chem. Soc.* **1948**, *70*, 99.

[7] H. Noel, J. Y. Le Marouille, *J. Solid State Chem.* **1984**, *52*, 197.

[8] B. Liang, L. Andrews, N. Ismail, C. J. Marsden, *Inorg. Chem.* **2002**, *41*, 2811–2813 (U + S₂).

[9] G. B. Jin, A. D. Raw, S. Skanthakumar, R. G. Haire, L. Soderholm, J. A. Ibers, *J. Solid State Chem.* **2010**, *183*, 547–550.

[10] X. F. Wang, L. Andrews, C. J. Marsden, *Inorg. Chem.* **2009**, *48*, 6888–6895 (U + SO₂).

[11] I. Infante, L. Andrews, X. F. Wang, L. Gagliardi, *Chem. Eur. J.* **2010**, *16*, 12804–12807.

[12] W. R. Wadt, *J. Am. Chem. Soc.* **1981**, *103*, 6053–6057.

[13] K. Tatsumi, I. Matsubara, Y. Inoue, A. Nakamura, R. E. Cramer, G. J. Tagoshi, J. A. Golen, J. W. Gilje, *Inorg. Chem.* **1990**, *29*, 4928–4938.

[14] G. D. Brabson, Z. Mielke, L. Andrews, *J. Phys. Chem.* **1991**, *95*, 79–86 (S₃ and S₄ in solid argon).

[15] a) J. P. Perdew, K. Burke, M. Ernzerhof, *Phys. Rev. Lett.* **1996**, *77*, 3865; b) C. Adamo, V. Barone, *J. Chem. Phys.* **1999**, *110*, 6158.

[16] a) B. O. Roos, P. R. Taylor, P. E. M. Siegbahn, *Chem. Phys.* **1980**, *48*, 157–173; b) P. E. M. Siegbahn, A. Heilberg, B. O. Roos, B. Levy, *Phys. Scr.* **1980**, *21*, 323–327; c) P. E. M. Siegbahn, A. Heilberg, J. Almlöf, B. O. Roos, *J. Chem. Phys.* **1981**, *74*, 2384–2397.

[17] a) K. Andersson, P.-Å. Malmqvist, B. O. Roos, A. J. Sadlej, K. Wolinski, *J. Phys. Chem.* **1990**, *94*, 5483–5488; b) K. Andersson, P.-Å. Malmqvist, B. O. Roos, *J. Chem. Phys.* **1992**, *96*, 1218–1227.

[18] R. D. Shannon, C. T. Prewitt, *Acta Crystallogr., Sect. B* **1969**, *25*, 925.

[19] R. C. L. Mooney-Slater, *Z. Kristallogr. Kristallgeom. Kristallphys. Kristallchem.* **1964**, *120*, 278.

[20] a) T. Ziegler, A. Rauk, *Inorg. Chem.* **1979**, *18*, 1558–1565; b) T. Ziegler, A. Rauk, *Theor. Chim. Acta* **1977**, *46*, 1–10.

[21] B. Liang, L. Andrews, *J. Phys. Chem. A* **2002**, *106*, 4038–4041 (Th + S₂).

[22] L. Andrews, H.-G. Cho, *Organometallics* **2006**, *25*, 4040–4053, and references cited therein.

[23] a) M. Douglas, N. M. Kroll, *Ann. Phys.* **1974**, *82*, 89–155; b) B. A. Hess, *Phys. Rev. A* **1986**, *33*, 3742–3748.

[24] a) B. O. Roos, R. Lindh, P.-Å. Malmqvist, V. Veryazov, P.-O. Widmark, *J. Phys. Chem. A* **2005**, *108*, 2851–2858; b) B. O. Roos, R. Lindh, P.-Å. Malmqvist, V. Veryazov, P.-O. Widmark, *Chem. Phys. Lett.* **2005**, *409*, 295–299.

[25] F. Aquilante, L. De Vico, N. Ferré, G. Ghigo, P.-Å. Malmqvist, P. Neogrády, T. B. Pedersen, M. Pitoňak, M. Reiher, B. O. Roos, L. Serrano-Andrés, M. Urban, V. Veryazov, R. Lindh, *J. Comput. Chem.* **2010**, *31*, 224–247.

[26] a) I. Infante, E. Eliav, M. J. Vilkas, Y. Ishikawa, U. Kaldor, L. Visscher, *J. Chem. Phys.* **2007**, *127*, 124308; b) F. Ruipérez, B. O. Roos, Z. Barandiarán, L. Seijo, *Chem. Phys. Lett.* **2007**, *434*, 1–5; c) F. Ruipérez, Z. Barandiarán, L. Seijo, *J. Chem. Phys.* **2007**, *127*, 144712; d) F. Ruipérez, C. Danilo, F. Réal, J.-P. Flament, V. Vallet, U. Wahlgren, *J. Phys. Chem. A* **2009**, *113*, 1420–1428; e) I. Infante, A. Kovacs, G. La Macchia, A. R. M. Shahi, J. K. Gibson, L. Gagliardi, *J. Phys. Chem. A* **2010**, *114*, 6007–6015; f) B. B. Averkiev, M. Mantina, R. Valero, I. Infante, A. Kovacs, D. G. Truhlar, L. Gagliardi, *Theor. Chem. Acc.* in press; g) F. Ruipérez, U. Wahlgren, *J. Phys. Chem. A* **2010**, *114*, 3615–3621.

[27] a) G. te Velde, F. M. Bickelhaupt, S. J. A. van Gisbergen, C. Fonseca Guerra, E. J. Baerends, J. G. Snijders, T. Ziegler, *J. Comput. Chem.* **2001**, *22*, 931–967; b) C. Fonseca Guerra, J. G. Snijders, G. te Velde, E. J. Baerends, *Theor. Chem. Acc.* **1998**, *99*, 391–403.